Polyamidoamine Dendrimers as Crosslinkers for Efficient Electron Transfer between Redox Probes onto Magnetic Nanoparticles

Feixiong Chen, Naoufel Haddour, Marie Frénéa-Robin, Yann Chevolot, Virginie Monnier

Polyamidoamine Dendrimers as Crosslinkers for Efficient Electron Transfer between Redox Probes onto Magnetic Nanoparticles

Feixiong Chen,[a] Naoufel Haddour,[b] Marie Frenea-Robin,[c] Yann Chevolot,[a] Virginie Monnier*[a]

[a] Dr. F. Chen, Dr. Y. Chevolot, Dr. V. Monnier
Université de Lyon, Institut des Nanotechnologies de Lyon (INL), UMR CNRS 5270, Site Ecole Centrale de Lyon, 36 Avenue Guy de Collongue, F-69134 Ecully Cedex, France.
E-mail : virginie.monnier@ec-lyon.fr

[b] Dr. N. Haddour
Université de Lyon, Ecole Centrale de Lyon, CNRS, UMR 5005, Laboratoire Ampère, Ecully, F-69130, France.

[c] Dr. M. Frenea-Robin
Université de Lyon, Université Lyon 1, CNRS, UMR 5005, Laboratoire Ampère, Villeurbanne, F-69622, France.

Abstract

The efficient conjugation of ferrocenecarboxylic acid (Fc), a usual electroactive probe, onto COOH-modified magnetic nanoparticles (NPs) is reported. Amine crosslinkers were used to couple COOH groups from NPs and from Fc. The coupling efficiencies using different generations of polyamidoamine (PAMAM) dendrimer and ethylenediamine (EDA) were compared through zeta potential measurements, square-wave voltammetry (SWV) and NH_2 titration. Highest PAMAM generations led to NH_2-modified NPs with increased zeta potential and NH_2 density compared to lowest ones. Moreover, no aggregation was observed after

crosslinker grafting. SWV was applied to characterize Fc-modified NPs. PAMAM generations 0-3 improved the electrochemical signal in comparison to EDA. However, increasing PAMAM generations led to NPs aggregation. Quantitative results supported the fact that PAMAM generation 0 was the best compromise for large electrochemical signal without NPs aggregation.

1. Introduction

Magnetic nanoparticles (NPs) are attracting considerable attention because of their high surface-to-volume ratio and their nanosize. Their unique superparamagnetic properties offer the possibility to manipulate them under an external magnetic field:[1–3] their huge magnetic moment causes them to move rapidly in the applied field and as they show no remanence, they fully disperse once the field is removed. Therefore, they are widely used in several kinds of biological applications such as bioseparation,[4] cell sorting,[5–7] biosensing,[8,9] drug delivery, [10] hyperthermia therapy[11] and cell imaging.[12] The implementation of surface modification protocols is fundamental to provide functional properties to these NPs. Magnetic NPs can be functionalized with different kinds of biomolecules such as antibodies,[8] oligonucleotides,[7] carbohydrates[15] or enzymes,[16] depending on the targeted application. However, other ligands with additional physico-chemical properties such as redox probes,[17–19] fluorescent dyes,[20,21] gold colloids[22,23] or quantum dots[24,25] can also be immobilized onto magnetic NPs.

Several strategies can be applied for magnetic NPs surface functionalization: physical adsorption, affinity-based or covalent bonding.[26] Among these methods, covalent bonding provides the best stability. In particular, carbodiimide coupling chemistry is widely used to form amide bonds between carboxylic acids and amines. As a carbodiimide reagent, 1-ethyl-3-(dimethylaminopropyl) carbodiimide hydrochloride (EDC) is the most commonly used as it is considered as a zero-length carboxyl-to-amine crosslinker, avoiding the increase of NPs hydrodynamic diameter during the functionalization process.

However, the number of biomolecules or ligands that can be immobilized is limited by the density of chemical reacting groups onto NPs surface. An interesting approach is to use dendrimer structures to increase the number of available chemical groups. Indeed, these fractal molecules can provide increasing amounts of functional groups with increasing generations. Polyamidoamine (PAMAM) dendrimers of different generations are suitable for carboxylate-modified NPs using carbodiimide chemistry. In previous studies, PAMAM dendrimers were either grafted[27] or built step by step[28–30] onto iron oxide NPs or other kinds of NPs such as silica[31] or quantum dots.[32]

This work reports on the functionalization of carboxy-modified magnetic NPs with PAMAM dendrimers of different generations derived from the same ethylenediamine (EDA) core. PAMAM generations from 0 to 3 (PAMAM-0, PAMAM-1, PAMAM-2 and PAMAM-3) and EDA were used for NPs functionalization. The resulting amine-modified NPs (NPs@EDA and NPs@PAMAM) were first characterized by zeta potential, NH_2 density and hydrodynamic diameter measurements. Then they were chemically modified with an electroactive molecule, ferrocene carboxylic acid (Fc). Voltammetry was used to evaluate the electrochemical signal while hydrodynamic diameter of Fc-modified NPs (NPs@EDA@Fc and NPs@PAMAM@Fc) was characterized by dynamic light scattering. Finally, a quantitative analysis of the reactivity of Fc electroactive molecules onto amine-modified NPs was performed. The average distance between two crosslinker molecules was determined with a core-shell model for PAMAM-modified NPs using data obtained from NH_2 colorimetric titration. Finally, the percentage of reactive NH_2 groups for Fc conjugation was deduced from voltammetry measurements, leading to hypotheses concerning electron transfer mechanism onto the surface of Fc-modified NPs.

2. Results and discussion

Initial magnetic NPs of 300 nm in diameter were composed of iron oxide nanoparticles embedded in COOH-modified polystyrene. Their surface modification process involves two steps as shown in Scheme 1: i) the grafting of amine-containing molecules onto initial carboxylic groups (NH_2-modified NPs) and ii) the conjugation of ferrocenecarboxylic acid (Fc-conjugated NPs). Both grafting steps were achieved via EDC coupling chemistry. After the first step of functionalization, amine groups provided by EDA molecule or PAMAM dendrimers from different generations were used to covalently conjugate Fc redox probes.

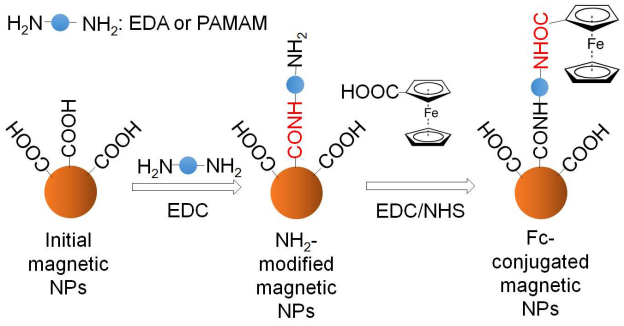

Scheme 1. *Illustration of the surface modification process of magnetic nanoparticles.*

2.1 Zeta potential, amine density and hydrodynamic diameter of NH_2-modified NPs

Zeta potential measurements, amine CBB titration and infrared spectroscopy of NH_2-modified NPs were first performed to evaluate the efficiency of the first functionalization step. Figure 1 and Figure 2 displayed zeta potential and amine density of the initial COOH-modified and the NH_2-modified NPs, respectively. PAMAM generation 0 to 3 modified NPs are called hereafter NPs@PAMAM-O, NPs@PAMAM-1, NPs@PAMAM-2, NPs@PAMAM-3, respectively. NPs@EDA stands for EDA-modified NPs.

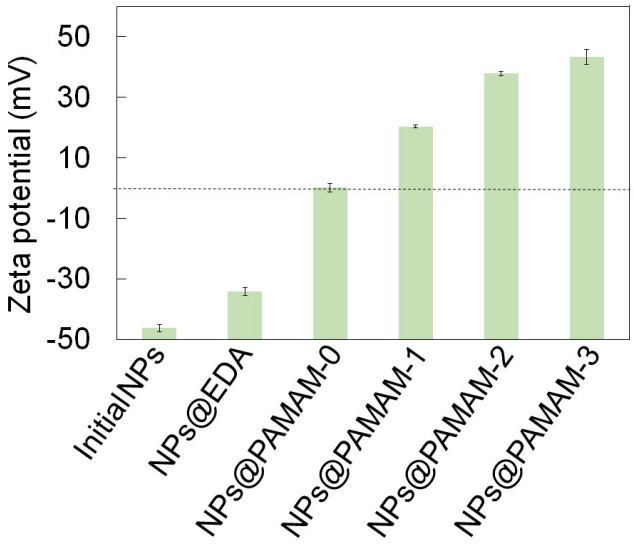

Figure 1. *Zeta potential of NH_2-modified nanoparticles with EDA and PAMAM dendrimers from different generations (measurement done in deionized water, pH = 6). Standard deviations were calculated as three independent experiments.*

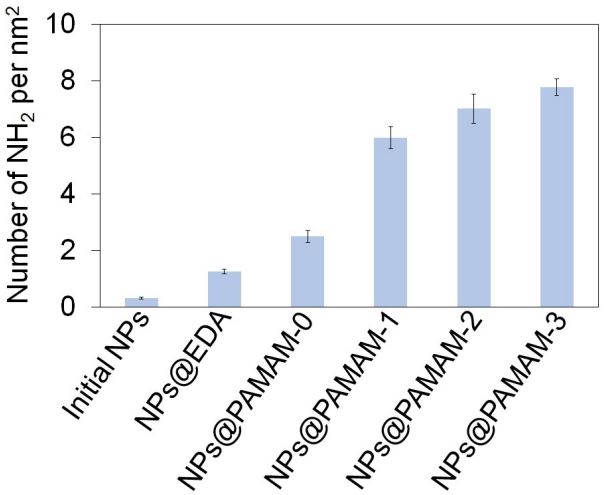

Figure 2. *Amine density of NH_2-modified nanoparticles with EDA and PAMAM dendrimers from different generations (obtained from CBB colorimetric titration). Standard deviations were calculated as three independent experiments.*

The zeta potential of the initial NPs bearing only carboxylic acids groups on their surface was measured to be -46.2 ± 1.1 mV with an amine density of 0.30 ± 0.03 NH_2 groups per nm^2. Indeed, in deionized water (pH = 6), these COOH groups are mostly dissociated into COO^- groups which contribute to the negative surface charge of NPs. The low amine density found can be attributed to nonspecific adsorption of CBB molecules onto NPs surface. After EDA grafting, zeta potential of NPs was increased to -34.2 ± 1.3 mV due to the positively charged NH_3^+ groups from the grafted EDA molecules. Indeed, as EDA contains only two NH_2 groups with one of them involved in an amide bond with COOH groups from NPs, the density of NH_2 groups onto NPs was found to be 1.25 ± 0.08 NH_2 groups per nm^2, corresponding to 0.95 ± 0.05 groups per nm^2 after substraction of the nonspecific adsorption, which is quite low. As a result, it is probable that there are still a majority of available COO^- groups, leading to a negative zeta potential. After PAMAM grafting, zeta potential increased significantly to 0.2 ± 1.4, 20.4 ± 0.4, 37.9 ±0.7 and 43.3 ± 2.4 mV for generations 0, 1, 2 and 3, respectively. Similarly, the amine density increased to 2.48 ± 0.22, 5.99 ± 0.39, 7.01 ± 0.52 and 7.78 ± 0.29 NH_2 groups per nm^2, respectively. This corresponds to 2.18 ± 0.19, 5.69 ± 0.36, 6.71 ± 0.49 and 7.48 ± 0.26 NH_2 groups per nm^2 after substraction of the nonspecific adsorption of CBB, respectively. Wang *et al* studied PAMAM dendrimers from several generations built *in situ* onto aminosilane-modified iron oxide NPs and calculated the number of NH_2 groups per NP from weight losses measurements.[30] Knowing the mean diameter of these NPs (11 nm), the amine density can be deduced and directly compared to our results. It showed that in this work, aminosilane-modified NPs have an amine density of 0.32 NH_2 groups per nm^2, which is three times lower than what was obtained for NPs@EDA. Then, they synthesized PAMAM generations 0, 1 and 2 directly onto the iron oxide NPs. It led to amine densities of 0.64, 1.3 and 2.6 NH_2 groups per nm^2, respectively, which is still nearly three times lower than the densities obtained in our work. Our results suggest that NPs@PAMAM present a higher NH_2

density than NPs@EDA and that higher PAMAM generations can provide higher NH_2 densities on the NPs, with more positive charges from NH_3^+ groups than negative charges caused by free COO^- groups. This is in agreement with previous work from Khodadust *et al*[29] that reported on PAMAM-functionalized silica-coated magnetic NPs using a dendronization process. In this case, a zeta potential sign change from a negative to a positive value was observed after PAMAM growth, associated to increasing nitrogen and carbon contents. An increasing nitrogen content with increasing PAMAM generations was also observed by Wang *et al*[30] on iron oxide NPs. In addition, Mitcova *et al*[27] also reported surface modification of COOH-terminated MNPs with different maleimide-terminated dendrimers. Similarly to our results, a zeta potential increase was observed after dendrimer grafting. A high density of maleimide groups available onto NPs surface was reported. As shown in Supporting Information (Figure S1 and Table S1), the number of NH_2 groups from EDA (PAMAM core) to PAMAM generation 3 is increased by a factor 16. However, the amine density was only multiplied by a factor of 6.2 from NPs@EDA to NPs@PAMAM-3. This difference could be first explained by the fact that one or more NH_2 groups of PAMAM dendrimers may be involved into amide bonds with initial COOH groups from NPs. Another explanation could be that, due to the dendritic structure, some NH_2 groups may not be accessible to CBB molecules during amine titration. Alternatively, it could also be that, as the number of amines increases on the surface of NPs, the increasing zeta potential tends to reduce the immobilisation yield by electrostatic repulsion. Finally, the grafting of PAMAM dendrimers onto NPs was also confirmed by infrared spectroscopy (Figure S2, Supporting Information). Indeed, compared to initial NPs, a new peak located at 1650 cm^{-1} was observed next to the stretching vibration of C=O located at 1730 cm^{-1} for NPs@PAMAM-0: this peak can be attributed to the stretching vibration of amide bonds from PAMAM dendrimer.

Aggregation of NPs must also be controlled and avoided during NH_2 functionalization. In order to evaluate the aggregation level, the hydrodynamic diameter of NH_2-modified NPs with EDA and different PAMAM generations was investigated by dynamic light scattering (Figure 3). The results suggest that all NH_2-modified NPs have similar hydrodynamic diameters than the starting COOH-modified NPs suggesting that NH_2-modified NPs dispersions are stable in water (pH approximately equal to 6), even NPs@PAMAM-0 which have a zeta potential value close to zero. Indeed, due to their initial negatively-charged shell, magnetic NPs are initially well dispersed and showed no aggregation when dispersed in water. PAMAM grafting induces a partial replacement of COO^- groups by NH_3^+ groups. The continuous presence of electrically charged chemical groups ensure a good dispersibility of magnetic NPs during PAMAM functionalization process. The zeta potential value close to zero obtained for NPs@PAMAM-0 suggest that COO^- negative charges are balanced (compensated) by the positive charge of NH_3^+ groups onto NPs surface. As shown in Figure 3, increasing PAMAM generations have no effect on NPs hydrodynamic diameter, due to the low diameter of PAMAM crosslinkers (3.6 nm for PAMAM-3 as shown in Table S1 in Supporting Information) compared to the diameter of magnetic NPs (300 nm). In the previous work of Wang *et al*,[30] a significant decrease of hydrodynamic diameter was observed after PAMAM grafting because initial magnetic NPs synthesized by coprecipitation were initially free of any stabilizing ligand.

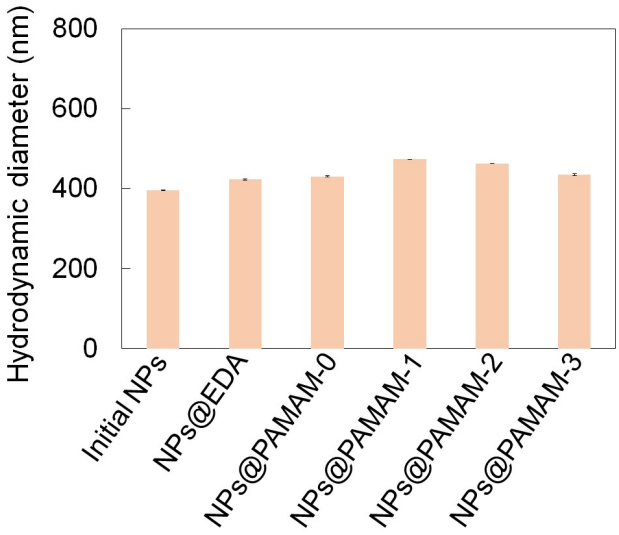

Figure 3. *Hydrodynamic diameters of initial and NH_2-modified magnetic nanoparticles with EDA and PAMAM dendrimers (measurement done in deionized water, pH = 6). Standard deviations were calculated as three independent experiments.*

2.2 Electrochemical measurement and hydrodynamic diameter of NPs@EDA@Fc and NPs@PAMAM@Fc

The NH_2-modified NPs were then conjugated to Fc by EDC/NHS chemistry. The resulting Fc-conjugated NPs were then characterized by infrared spectroscopy and voltammetry to evaluate the efficiency of Fc conjugation onto PAMAM-modified NPs. As shown in Figure S2 (Supporting Information), infrared spectrum of NPs@PAMAM-0@Fc is characterized by the presence of a new large band located around 1010 cm^{-1}, which may be related to the asymmetric vibration of C=C bonds of cyclopentadienyl ring from ferrocene. As a negative control, an infrared spectrum of NPs@PAMAM-0 in presence of unactivated Fc (without the use of EDC/NHS) was also acquired. In this case, the large band at 1010 cm^{-1} was not observed. Using voltammetry, it must be noted that only Fc submitted to the redox reaction can be detected. Figure S3 (Supporting Information) displays the SWV curves of Fc-conjugated NPs using EDA and different PAMAM generations as chemical linkers after elimination of background signal. The presence of an anodic current peak on SWV curves undoubtedly confirmed the presence

of Fc redox probe at the surface of Fc-conjugated NPs in comparison to the two negative controls: NH_2-modified NPs and NH_2-modified NPs reacted with unactivated Fc. As shown in Figure 4, all Fc-conjugated NPs prepared with PAMAM dendrimer crosslinkers showed higher peak currents than those prepared with EDA.

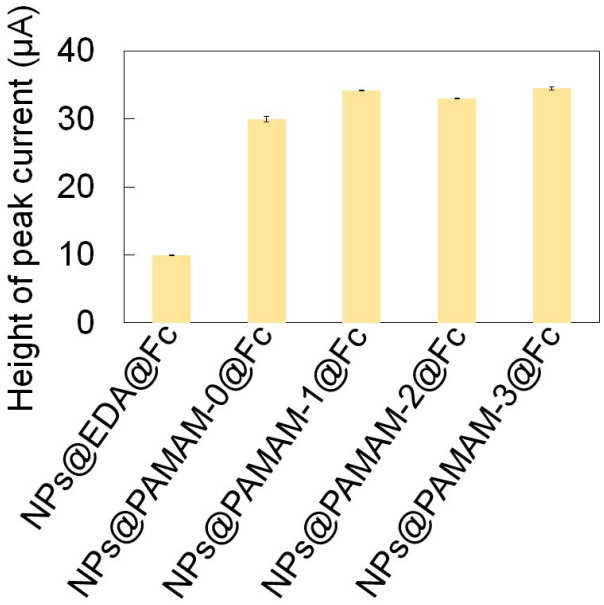

Figure 4. *SWV peak current height for Fc-conjugated nanoparticles (300 µg mL^{-1} in PBS 1X) using EDA and PAMAM as chemical linkers. Standard deviations were calculated as three independent experiments.*

Nevertheless, the electrochemical current density of Fc-conjugated NPs was not improved with increasing PAMAM generations. Moreover, dynamic light scattering measurements suggested that aggregation occurred for NPs@PAMAM-1@Fc, NPs@PAMAM-2@Fc and NPs@PAMAM-3@Fc (Figure 5) for which the average hydrodynamic diameter was over 1 µm. On the contrary, this diameter remained close to that of the initial NPs (Figure 3) for NPs@EDA@Fc and NPs@PAMAM-0@Fc. The replacement of NH_2 groups from PAMAM by Fc may explain the aggregation of NPs due to the reduction of the density of charged chemical groups onto NPs surface.

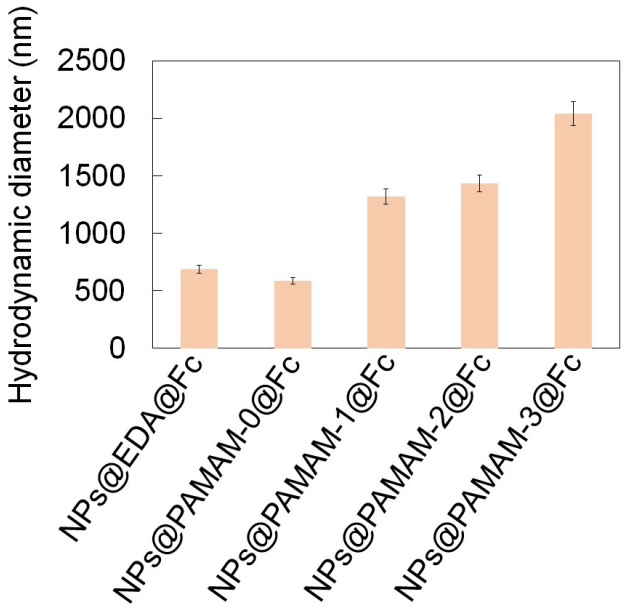

Figure 5. *Hydrodynamic diameter of Fc-conjugated nanoparticles with EDA and PAMAM dendrimer (measurement done in PBS 1X, pH = 7.4). Standard deviations were calculated as three independent experiments.*

2.3 Quantitative analysis of the reactivity of Fc electroactive molecules onto NH_2-modified NPs

To better understand how the crosslinker choice affects the reactivity of Fc and consequently the resulting electrochemical signal, a quantitative analysis was performed. From the intrinsic characteristics of amine crosslinkers (Table S1, Supporting Information) and the measured data (NH_2 density onto NPs, Figure 2), it was possible to evaluate the average distance between 2 crosslinker molecules after their immobilization onto the NPs surface. In order to perform this calculation, a core-shell model was designed for NPs, with a core composed of initial magnetic NPs and a shell composed of crosslinker molecules (Scheme 2). This kind of model was already selected by other groups to study the structure of NPs coated with polyethylene glycol (PEG) molecules [33–35]: the extracted parameters were the molecules volume density inside the shell, the shell thickness and the spacing distance between PEG at the surface of NPs.

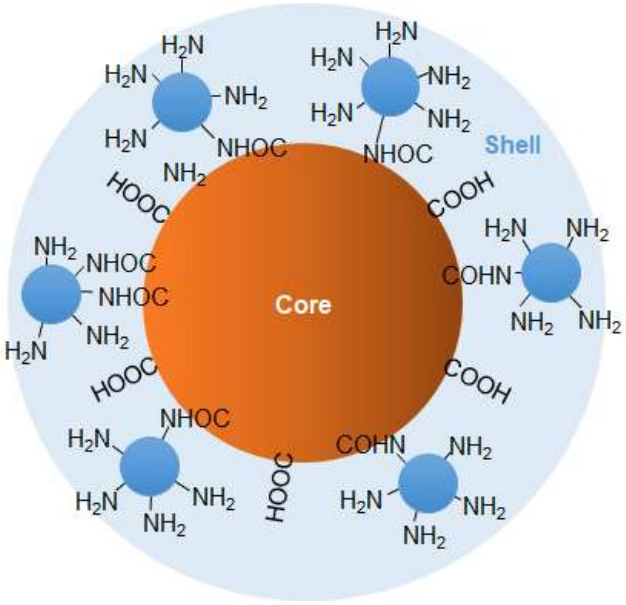

Scheme 2. *Core-shell model for the determination of average distance between crosslinkers onto NPs surface. Core is composed of initial magnetic NPs and a shell composed of crosslinker (EDA or PAMAM) molecules.*

In our work, the core-shell model was studied as follow. On one hand, from the diameters of the different crosslinkers (named CL in Table 1) shown in Supporting Information (Table S1) and the surface of one NP of 300 nm in diameter, it is possible to estimate the volume of the shell developed by these crosslinkers when immobilized onto NPs surface. On the other hand, amine group titration with CBB, as reported in Figure 2, can be used to determine the amine volume density inside the shell. As the number of amine groups per crosslinker is known (Table S1, Supporting Information), the crosslinker density inside the shell can be deduced. To achieve this, it was considered that at least one amine group from each crosslinker was involved into an amide bond with NP surface and that at most, half of these amine groups were involved into amide bonds. The calculation results are presented in Table 1.

Table 1. *Evaluation of the average distance between two crosslinker (CL) molecules after their immobilization onto NP surface.*

Crosslinker (CL)	Volume of CL shell (nm^3)*	Number of reactive NH_2 groups per CL**	NH_2 density onto NPs surface (nm^{-2})***	Number of NH_2 inside the CL shell for 1 NP****	Number of CL per NP	CL density inside the shell (nm^{-3})	Average distance between two CL (nm)
EDA	1.2×10^5	1	0.95	2.7×10^5	2.7×10^5	2.2	0.1
PAMAM-0	4.2×10^5	2-3	2.18	6.2×10^5	2.1×10^5-3.1×10^5	0.48-0.73	2.6-8.8
PAMAM-1	6.2×10^5	4-7	5.69	16×10^5	2.3×10^5-4.0×10^5	0.37-0.64	3.7-20
PAMAM-2	8.2×10^5	8-15	6.71	19×10^5	1.3×10^5-2.4×10^5	0.15-0.29	41-272
PAMAM-3	10×10^5	16-31	7.48	21×10^5	0.7×10^5-1.3×10^5	0.07-0.13	457-3320

* The surface of a 300 nm diameter NP is 282600 nm^2. The volume of CL shell is the CL diameter (Table S1, Supporting Information) multiplied by this surface.
** Free NH_2 groups not involved in amide bonds with COOH groups from initial NPs (number of NH_2 groups per CL molecule given in Table S1, Supporting Information).
*** Values obtained from CBB titration (Figure 2) after substraction of the nonspecific adsorption level of CBB (0.30 nm^{-2}) corresponding to the amine density measured onto initial NPs.
**** estimated from ***.

The average distance between two chemical linkers is very low for EDA, suggesting that EDA molecules form a dense layer at the surface of NPs. This result could seem contradictory with the negative zeta potential value (-34.2 mV) of NPs@EDA, as shown in Figure 1. However, as a small molecule, the average distance between 2 EDA molecules taking into account only the surface density of 0.95 EDA per nm^2, would give an average distance of 1.1 nm. This value is also consistent with a dense EDA layer. This could be explained by the very high surface density of COOH groups onto initial magnetic NPs (14 COOH per nm^2, giving an average distance of 0.005 nm) due to the polymeric nature of the initial shell of NPs. Thus, the initial surface of NPs could be considered as a porous structure in which even a low functionalization level gave rise to high surface density of modified chemical functions. Concerning PAMAM crosslinkers, this distance becomes larger and increases with increasing PAMAM generations. The same evolution was obtained by Minelli *et al* for PEG-modified gold NPs.[35] However, the study of molecule spacing distance as a function of PEG molecular weight gave a cube root dependence

which was not the case in our work (Figure S4, Supporting Information). For PAMAM-3, the extremely high value of 3320 nm between two molecules is probably overestimated due to the fact that it is highly improbable that PAMAM-3 would be linked by only one NH_2 group to the surface of NP. However, this large distance may influence the electrochemical signal obtained after Fc immobilization. Indeed, electron transfer between electroactive molecules can be significantly accelerated due to electron hopping.[36] This process strongly depends on the average distance between molecules which has generally to be lower than 2 nm[37] although it can be increased up to 5 nm in systems with the inclusion of NPs.[38] Due to crosslinker low diameters (Table S1, Supporting Information), Fc molecules anchored onto the same crosslinker molecule are probably submitted to electron hopping. On the contrary, due to the large intermolecular distance between crosslinkers on the surface of NPs (Table 1), there is probably no electron hopping between Fc molecules when they are located on different crosslinker molecules except when EDA and PAMAM-0 are used. This could explain why SWV peak currents reached a plateau from NPs@PAMAM-1@Fc to NPs@PAMAM-3@Fc (Figure 4). In this case, electron transfer cannot exist on the whole Fc molecules immobilized onto NPs surface, leading to an underestimation of their electrochemical signal. Another explanation could be that dendrimers of increasing generations block the electron transfer between Fc molecules and working electrode. This was observed for ferrocene-modified gold nanoparticles deposited onto electrodes coated with PAMAM dendrimers.[39]

Finally, as negligible aggregation is observed for NPs@EDA@Fc and NPs@PAMAM-0@Fc (as shown in Figure 5), it may be assumed that the area of anodic peak current (Figure S3, Supporting Information), is related to the number of Fc molecules immobilized onto NPs. Thus, it is possible to estimate the number of reactive NH_2 groups from EDA and PAMAM-0 that were used for Fc conjugation. Table 2 summarized the quantification results obtained from these two kinds of NPs.

Table 2. *Evaluation of the percentage of reactive NH_2 groups for Fc conjugation using EDA and PAMAM-0 as crosslinkers.*

Crosslinker (CL)	Number of NH_2 groups per nm^2*	Anodic surface charge (µC)***	Number of Fc molecules per nm^2	Percentage of reactive NH_2 groups for Fc conjugation***
EDA	0.95 ± 0.08	41.27 ± 1.38	0.172 ± 0.0058	18.1 %
PAMAM-0	2.18 ± 0.22	142.51 ± 2.11	0.594 ± 0.0089	27.2 %

* Values obtained from CBB titration (Figure 2) after subtraction of the nonspecific adsorption level of CBB (0.30 nm^{-2}) corresponding to the amine density measured onto initial NPs.
** The anodic surface charge was calculated from the area under SWV curves after background subtraction (Figure S2, Supporting Information).
*** The percentage of reactive NH_2 groups for Fc conjugation was obtained from the ratio between the number of Fc molecules per nm^2 and the number of NH_2 groups per nm^2.

The percentages of reactive NH_2 groups for Fc conjugation were deduced from the ratio between Fc molecules density and NH_2 group density. This percentage was calculated to be 18.1 % and 27.2 % for NPs@EDA@Fc and NPs@PAMAM-0@Fc, respectively. This supports the better reactivity of NH_2 groups onto PAMAM-0 compared to EDA molecule. The higher number of degrees of freedom of NH_2 groups on PAMAM-0 compared to EDA can explain their better reactivity. Moreover, as the Fc surface density is improved for NPs@PAMAM-0@Fc compared to NPs@EDA@Fc, faster electron transfer can be expected. This is consistent with previous works[40] about ferrocene-terminated monolayers onto silicon surface, showing that the surface coverage of ferrocene directly influences the charge transfer rate with a linear relationship. Indeed, a surface coverage of ferrocene higher than 5×10^{-11} mol cm^{-2} seems to be critical to allow an efficient charge transfer between ferrocene molecules. It was also shown that self-assembled monomayers of PAMAM dendrimers onto electrodes surface favour redox shuttling because of pinholes or nanopores between dendrimer molecules. In our work, the Fc surface density of 0.172 and 0.594 Fc molecules per nm^{-2}, corresponding to 2.8×10^{-11} and 1×10^{-10} mol cm^{-2}, for NPs@EDA@Fc and NPs@PAMAM-0@Fc, respectively, are consistent with an efficient charge transfer only occurring for NPs@PAMAM-0@Fc. This possibility to get electron hopping between Fc molecules on the whole NP surface associated to the negligible

aggregation of resulting NPs, PAMAM-0 can be considered as the optimal crosslinker to immobilize Fc onto NP surface. Preliminary results about potential application of NPs@PAMAM-0@Fc as nanoprobes for glucose sensing are shown in Supporting Information (Figure S5).

3. Conclusions

In summary, carboxylic-modified magnetic NPs were successfully functionalized with amine containing molecules such as EDA and PAMAM dendritic structures (generations 0 to 3) via EDC coupling chemistry. NH_2-modified NPs displayed increasing zeta potential and higher amine density when using higher PAMAM generations and no aggregation was observed. Fc-conjugated NPs were also developed by efficient conjugation between Fc redox probe and NH_2-modified NPs, which were characterized by square-wave voltammetry. PAMAM-0 dendritic structure improved the electrochemical signal intensity of Fc-conjugated NPs in comparison to EDA molecule. Nevertheless, electrochemical signal intensity was not significantly improved using higher PAMAM generations (from 1 to 3). In addition, aggregation was observed for NPs@PAMAM-1@Fc, NPs@PAMAM-2@Fc and NPs@PAMAM-3@Fc, while EDA and PAMAM-0 led to low aggregation. A quantitative analysis also showed that the low intermolecular distance between EDA and PAMAM-0 molecules at the NPs surface allows the existence of electron hopping, leading to an enhanced electrochemical signal. Moreover, no aggregation was observed for these NPs. Finally, NH_2 groups located on PAMAM-0 were more reactive than NH_2 groups located on EDA. These magnetic NPs@PAMAM-0@Fc can be now considered as suitable starting building blocks to perform further functionalization steps, with a broad range of applications in biotechnology and biomedicine.

Supporting Information

Experimental details, characteristics of PAMAM dendrimer, infrared transmission spectra and SWV curves of NPs, average distance between CL molecules as a function of CL molecular weight can be found in the Supporting Information available online.

Acknowledgements

This work was supported by the BQR ('Bonus Qualité Recherche') of Ecole Centrale de Lyon. We are indebted to the Chinese Scholarship Council for the financial support of F. Chen.

Keywords: Magnetic nanoparticles, PAMAM dendrimer, ferrocene carboxylic acid, surface chemistry, electron transfer.

References

[1] R. H. Kodama, *J. Magn. Magn. Mater.* **1999**, *200*, 359–372.

[2] S. Chikazumi, S. Taketomi, M. Ukita, M. Mizukami, H. Miyajima, M. Setogawa, Y. Kurihara, *J. Magn. Magn. Mater.* **1987**, *65*, 245–251.

[3] A. H. Lu, E. L. Salabas, F. Schüth, *Angew. Chem., Int. Ed.* **2007**, *46*, 1222–1244.

[4] I. Yildiz, *Nanotechnol. Rev.* **2011**, *5*, 331–340.

[5] Y. Wang, C. Xu, H. Ow, *Theranostics* **2013**, *3*, 544–560.

[6] O. Osman, S. Toru, F. Dumas-Bouchiat, N. M. Dempsey, N. Haddour, L.-F. Zanini, F. Buret, G. Reyne, M. Frénéa-Robin, *Biomicrofluidics* **2013**, *7*, 54115.

[7] S. Bhana, Y. Wang, X. Huang, *Nanomedicine (London, U. K.)* **2015**, *10*, 1973–1990.

[8] J. B. Haun, T. J. Yoon, H. Lee, R. Weissleder, *Wiley Interdiscip. Rev. Nanomed.*

Nanobiotechnol. **2010**, *2*, 291–304.

[9] D. Issadore, Y. I. Park, H. Shao, C. Min, K. Lee, M. Liong, R. Weissleder, H. Lee, *Lab Chip* **2014**, *14*, 2385.

[10] L. Zhu, Z. Zhou, H. Mao, L. Yang, *Nanomedicine (London, U. K.)* **2017**, *12*, 73–87.

[11] S.-H. Noh, S. H. Moon, T. H. Shin, Y. Lim, J. Cheon, *Nano Today* **2017**, *13*, 61–76.

[12] Z. Shen, A. Wu, X. Chen, *Mol. Pharmaceutics* **2017**, *14*, 1352–1364.

[13] J. R. McCarthy, R. Weissleder, *Adv. Drug Delivery Rev.* **2008**, *60*, 1241–1251.

[14] M. Trévisan, M. Schawaller, G. Quapil, E. Souteyrand, Y. Mérieux, J.-P. Cloarec, *Biosens. Bioelectron.* **2010**, *26*, 1631–1637.

[15] Y. S. Raval, B. D. Fellows, J. Murbach, Y. Cordeau, O. T. Mefford, T. R. J. Tzeng, *Adv. Funct. Mater.* **2017**, *27*, 1–11.

[16] Y. Zhou, S. Pan, X. Wei, L. Wang, Y. Liu, *BioResources* **2013**, *8*, 2605–2619.

[17] H. Li, Q. Wei, J. He, T. Li, Y. Zhao, Y. Cai, B. Du, Z. Qian, M. Yang, *Biosens. Bioelectron.* **2011**, *26*, 3590–3595.

[18] X. Zhu, J. Li, H. Lv, H. He, H. Liu, X. Zhang, S. Wang, *RSC Adv.* **2017**, *7*, 36124–36131.

[19] S. Du, Y. Luo, F. Zuo, X. Li, D. Liu, *Nano* **2017**, *12*, 1750037.

[20] C. Kaewsaneha, P. Tangboriboonrat, D. Polpanich, A. Elaissari, *ACS Appl. Mater. Interfaces* **2015**, *7*, 23373–23386.

[21] S. D. Topel, Ö. Topel, R. B. Bostancioğlu, A. T. Koparal, *Colloids Surf., B* **2015**, *128*, 245–253.

[22] S. Moraes Silva, R. Tavallaie, L. Sandiford, R. Tilley, J. J. Gooding, *Chem. Commun.* **2016**, *52*, 7528–7540.

[23] D. K. Lee, Y. Song, V. T. Tran, J. Kim, E. Y. Park, J. Lee, *J. Colloid Interface Sci.* **2017**, *499*, 54–61.

[24] S. Mohapatra, S. Sahu, S. Nayak, S. K. Ghosh, *Langmuir* **2015**, *31*, 8111–8120.

[25] L. Moro, M. Turemis, B. Marini, R. Ippodrino, M. T. Giardi, *Biotechnol. Adv.* **2017**, *35*, 51–63.

[26] R. A. Sperling, W. J. Parak, *Philos. Trans. R. Soc., A* **2010**, *368*, 1333–1383.

[27] L. Mitcova, H. Rahma, T. Buffeteau, R. Clérac, L. Vellutini, K. Heuzé, *RSC Adv.* **2015**, *5*, 88574–88577.

[28] R. Abu-Reziq, H. Alper, D. Wang, M. L. Post, *Drug Discovery Today* **2006**, *128*, 5279–5282.

[29] R. Khodadust, G. Unsoy, S. Yalcın, G. Gunduz, U. Gunduz, *J. Nanopart. Res.* **2013**, *15*, 1488.

[30] T. Wang, W. L. Yang, Y. Hong, Y. L. Hou, *Chem. Eng. J.* **2016**, *297*, 304–314.

[31] H. Yamaguchi, M. Tsuchimochi, K. Hayama, T. Kawase, N. Tsubokawa, *Int. J. Mol. Sci.* **2016**, *17*, 1086.

[32] W. Tang, Y. Wang, P. Wang, J. Di, J. Yang, Y. Wu, *Microchim. Acta* **2016**, *183*, 2571–2578.

[33] A. Ramzi, C. J. F. Rijcken, T. F. J. Veldhuis, D. Schwann, W. E. Henninkj, C. F. Van Nostrum, *J. Phys. Chem. B* **2008**, *112*, 784–792.

[34] M. D. Torelli, R. A. Putans, Y. Tan, S. E. Lohse, C. J. Murphy, R. J. Hamers, *ACS Appl. Mater. Interfaces* **2015**, *7*, 1720–1725.

[35] C. Minelli, A. G. Shard, *Biointerphases* **2016**, *11*, 04B306.

[36] N. Papageorgiou, M. Gra, O. Enger, D. Bonifazi, F. Diederich, *J. Phys. Chem. B* **2002**, *106*, 3813–3822.

[37] J. P. Launay, *Chem. Soc. Rev.* **2001**, *30*, 386–397.

[38] F. Liu, K. Khan, J. H. Liang, J. W. Yan, D. Y. Wu, B. W. Mao, P. S. Jensen, J. Zhang, J. Ulstrup, *ChemPhysChem* **2013**, *14*, 952–957.

[39] P. P. Fang, O. Buriez, E. Labbé, Z. Q. Tian, C. Amatore, *J. Electroanal. Chem.* **2011**, *659*, 76–82.

[40] B. Fabre, *Acc. Chem. Res.* **2010**, *43*, 1509–1518.